Video Article

Longitudinal Measurement of Extracellular Matrix Rigidity in 3D Tumor Models Using Particle-tracking Microrheology

Dustin P. Jones*[1], William Hanna*[1], Hamid El-Hamidi[1], Jonathan P. Celli[1]

[1]Department of Physics, University of Massachusetts Boston

*These authors contributed equally

Correspondence to: Jonathan P. Celli at Jonathan.Celli@umb.edu

URL: http://www.jove.com/video/51302
DOI: doi:10.3791/51302

Keywords: Bioengineering, Issue 88, viscoelasticity, mechanobiology, extracellular matrix (ECM), matrix remodeling, 3D tumor models, tumor microenvironment, stroma, matrix metalloprotease (MMP), epithelial-mesenchymal transition (EMT)

Date Published: 6/10/2014

Citation: Jones, D.P., Hanna, W., El-Hamidi, H., Celli, J.P. Longitudinal Measurement of Extracellular Matrix Rigidity in 3D Tumor Models Using Particle-tracking Microrheology. *J. Vis. Exp.* (88), e51302, doi:10.3791/51302 (2014).

Abstract

The mechanical microenvironment has been shown to act as a crucial regulator of tumor growth behavior and signaling, which is itself remodeled and modified as part of a set of complex, two-way mechanosensitive interactions. While the development of biologically-relevant 3D tumor models have facilitated mechanistic studies on the impact of matrix rheology on tumor growth, the inverse problem of mapping changes in the mechanical environment induced by tumors remains challenging. Here, we describe the implementation of particle-tracking microrheology (PTM) in conjunction with 3D models of pancreatic cancer as part of a robust and viable approach for longitudinally monitoring physical changes in the tumor microenvironment, *in situ*. The methodology described here integrates a system of preparing *in vitro* 3D models embedded in a model extracellular matrix (ECM) scaffold of Type I collagen with fluorescently labeled probes uniformly distributed for position- and time-dependent microrheology measurements throughout the specimen. *In vitro* tumors are plated and probed in parallel conditions using multiwell imaging plates. Drawing on established methods, videos of tracer probe movements are transformed via the Generalized Stokes Einstein Relation (GSER) to report the complex frequency-dependent viscoelastic shear modulus, $G^*(\omega)$. Because this approach is imaging-based, mechanical characterization is also mapped onto large transmitted-light spatial fields to simultaneously report qualitative changes in 3D tumor size and phenotype. Representative results showing contrasting mechanical response in sub-regions associated with localized invasion-induced matrix degradation as well as system calibration, validation data are presented. Undesirable outcomes from common experimental errors and troubleshooting of these issues are also presented. The 96-well 3D culture plating format implemented in this protocol is conducive to correlation of microrheology measurements with therapeutic screening assays or molecular imaging to gain new insights into impact of treatments or biochemical stimuli on the mechanical microenvironment.

Video Link

The video component of this article can be found at http://www.jove.com/video/51302/

Introduction

It is clear from a growing body of evidence in the literature that cancer cells, as with non-malignant mammalian epithelial cells, are highly sensitive to the mechanical and biophysical properties of the surrounding extracellular matrix (ECM) and other microenvironment components[1-9]. Elegant mechanistic studies have provided insights into the role of extracellular rigidity as a complex mechanosensitive signaling partner that regulates malignant growth behavior and morphogenesis[2,3,10,11]. This work has been facilitated in particular by the development of 3D *in vitro* tumor models that restore biologically relevant tissue architecture and can be grown in scaffold materials with tunable mechanics and imaged by optical microscopy[12-19]. However, the other side of this mechanoregulatory dialog between tumor and microenvironment, through which cancer cells in turn modify the rheology of their surroundings, remains somewhat more difficult to study. For example, during invasion processes, cells at the periphery of a tumor may undergo epithelial to mesenchymal transition (EMT) and increase expression of matrix metalloproteases (MMPs) that cause local degradation of ECM[20-22], which in turn influences mechanosensitive growth behavior of other proximal tumor cells. Through a variety of biochemical processes, cancer cells continually dial the local rigidity of their environment up and down to suit different processes at different times. The methodology described here is motivated by the need for analytical tools that report local changes in the rigidity and compliance of the ECM during growth, that can be integrated with 3D tumor models and correlated longitudinally with biochemical and phenotypic changes without terminating the culture.

In search of an appropriate technique to implement in this context, particle-tracking microrheology (PTM) emerges as a strong candidate. This method, pioneered originally by Mason and Weitz[23,24], uses the motion of tracer probes embedded in a complex fluid to report the frequency-dependent complex viscoelastic shear modulus, $G^*(\omega)$ at micron length scales. This general approach has been developed with multiple variations suited for different applications in soft-condensed matter, colloids, biophysics and polymer physics[25-31]. PTM has certain advantages relative to other methods, since readouts of local viscoelasticity are provided by non-destructive video imaging of biochemically inactive tracer probes that are incorporated at the time of culture preparation and remain in place over extended periods of growth. This is in contrast to gold standard measurements with an oscillatory shear bulk rheometer, which necessarily requires termination of the culture and reports the bulk

macroscopic rheology of the sample rather than point measurements within the complex 3D tumor microenvironment. Indeed a number of studies have illustrated the utility of interpreting measurements of tracer probe movements in or around cancer or non-cancer cells to measure deformations associated with cell migration[32], mechanical stress induced by an expanding spheroid[33], intracellular rheology[34,35], and to map mechanical stresses and strains in engineered tissues[36], and relation between pore size and invasion speed[37]. Other techniques suitable for microrheology, such as atomic force microscopy (AFM) can be implemented, but primarily for probing points at the sample surface and also may pose culture sterility issues that complicate longitudinal measurements[38].

Here, we describe a comprehensive protocol encompassing methods for growth of 3D tumor spheroids suitable for transfer into ECM with embedded fluorescent probes for video particle-tracking and analysis methods for reliably mapping spatial changes in microrheology over time in culture. In the present implementation, 3D tumor models are grown in multiwell format with a view towards incorporation of microrheology measurements with other traditional assays (*e.g.*, cytotoxicity) which this format is conducive to. In this representative illustration of this methodology we culture *in vitro* 3D spheroids using PANC-1 cells, an established pancreatic cancer cell line known to form spheroids[39], but all measurements described herein are broadly applicable to study of solid tumors using a variety of cell lines suitable for 3D culture. Because this method is inherently imaging-based it is ideally suited for co-registration of high-resolution microrheology data with large transmitted-light fields of view that report changes in cell growth, migration and phenotype. The implementation of PTM integrated with transmitted light microscopy in this manner assumes reproducible positioning of the microscope stage which is typically available on motorized commercial widefield epifluorescence biological microscopes. The protocol developed below can be implemented with any reasonably equipped automated fluorescence biological microscope. This is an inherently data-intensive method, which requires acquisition of gigabytes of digital video microscopy data for offline processing.

In the following protocol, Protocol 1 pertains to the initial preparation of tumor spheroids which is described here using overlay on agarose but could be substituted with a variety of other methods such as hanging drop[40], or rotary culture[41] techniques. Protocol 2 describes the process of embedding spheroids in a collagen scaffold though alternatively, *in vitro* 3D tumors could be grown by encapsulation or embedding of resuspended cells in ECM[12,15], rather than single pre-formed non-adherent spheroids. Subsequent protocols describe procedures for obtaining time-resolved microrheology measurements by acquiring and processing video microscopy data, respectively. Data processing is described using MATLAB, making use of open source routines for PTM built on algorithms originally described by Crocker and Grier[42], which have also been extensively developed for different software platforms (see http://www.physics.emory.edu/~weeks/idl/).

Protocol

1. Culturing Tumor Spheroids

1. Mix 10 ml of cell culture grade water with 0.1 g of agarose to obtain a 1% agarose solution.
2. Heat agarose solution to above 70 °C (roughly 14 sec in a standard microwave or by using a heating plate) before aliquoting 40 µl of agarose solution into a well on a 96-well plate.
3. Incubate plate at 37 °C for at least 1 hr while harvesting cells using standard techniques.
4. Use a hemacytometer to determine the concentration of cells in the suspension.
5. Dilute cell suspension to 1,000 cells/ml and add 100 µl of this dilution to the well containing the cured agarose bed.
6. Place the sample on a shaker overnight in an incubator set at 37 °C and 5% CO_2.
7. Remove sample from shaker and add 100 µl of cell culture media.
8. Incubate spheroids until desired diameter is reached. For example, after 9 days, a spheroid will be approximately 450 µm in diameter. During this time, fresh growth media can be added to the wells but aspiration should be avoided since this will result in removal of the spheroid.

2. Preparing 3D Tumor Spheroids Embedded in ECM

1. Prepare a work station with needed materials inside a laminar flow hood.
2. Prepare a diluted mixture of carboxylate-modified 1 µm diameter fluorescent tracer probes by adding 2 parts stock probes (2% solids) to 25 parts sterile water.
3. Remove a bottle of 3.1 mg/ml bovine collagen from the refrigerator and place it on ice.
4. Aliquot 125 µl of collagen into an empty 2 ml vial.
5. Add 50 µl of diluted tracer probe solution to the vial containing the collagen and vortex briefly to distribute probes.
6. Add 235 µl of appropriate cell culture media containing phenol red (which will turn yellow) for a total volume of 410 ml and vortex briefly before removing 205 ml (half the total volume) and placing it in a new 2 ml vial. Vial 1 will contain the tumor spheroid and Vial 2 will be a control mixture.
7. Add ~2 µl of 1 M NaOH to Vial 1 to bring the solution back to neutral pH (culture media containing phenol red should return to red). Note that this will cause the mixture to begin curing if it is not kept on ice. Vortex briefly to mix, then return to ice rack immediately.
   NOTE: The spheroid is barely visible to the naked eye after 9 days of culture and its removal from the agarose bed is a delicate task. Use of a dissection microscope may be helpful for some users. Maintaining the integrity of the spheroid during transfer is paramount.
8. Using a wide-mouth pipette tip, gently remove 40 µl of media from the well containing the tumor spheroid. Retain this 40 µl while conducting the next step.
9. Check the well to see if the spheroid was removed in the previous step. If it was, add the 40 µl containing the spheroid to Vial 1. If not, place the 40 µl back into the well and repeat the previous step.
10. Gently stir Vial 1 (do not risk vortexing, it may damage the spheroid) before transferring the mixture in 60 µl portions into three separate wells of a 96-well plate. Inspect each well with a microscope after adding mixture to determine which well contains the spheroid.
11. Add ~2 µl 1 M NaOH and 40 µl of cell culture media to Vial 2 and vortex before aliquotting 60 µl of this mixture to an empty well in the 96-well plate and labeling as a control.
12. Place the plate in a 37 °C incubator to cure for at least 1 hr.

3. Construct Grid of Sample Points and Take a Video at Each Point

1. Transfer the sample plate from the incubator to the microscope stage. Allow 10 min for the sample to equilibrate with the room temperature if a heated stage is not available.
2. Observe the sample with low powered objective lenses to make sure it is intact and ready for imaging. Determine the tumor position within the well.
3. Decide how many sample points to take. Typically, 20 sample points in each well, distributed in concentric rings around the spheroid will produce adequately detailed results.
4. Move the stage to each desired position and use microscope interfacing software to record the x and y coordinates (or record coordinates manually if interfacing software is unavailable).
5. Switch the microscope to a high powered objective lens (typically 100X), and select the appropriate filter cube for the excitation wavelength of the tracer probes. Use the list of points created in step 3.4 to move to the first point in the grid.
6. Adjust the focus to find the bottom of the well, then move up to find a field of view (fov) containing several in-focus tracer probes.
7. Observe the intensity histogram and adjust the exposure intensity and time to give the greatest dynamic range possible while ensuring that the image does not become saturated.
8. Obtain a video sequence at a frame rate of 20-30 msec per frame (approximately 800 frames or 16-24 sec in length is recommended to provide sufficient statistics for robust MSD calculation balanced with the need for minimizing acquisition time at each spatial grid point) and save with an appropriate convention. During the recording, do not touch the microscope or table.
9. Repeat steps 3.6 to 3.9 for each sample point in the grid.
10. Repeat steps 3.3 to 3.10 for each well in the experiment.

4. Analyze Video Data to Compute Rheological Properties at Each Sample Point

1. Copy all video data to an analysis folder (possibly on a different computer).
2. Import image data into MATLAB or other analysis software.
   NOTE: Extensive documentation regarding the set of MATLAB particle tracking routines adopted here is available at http://people.umass.edu/kilfoil. The use of a custom calling function for automating processing of multiple files at different positions is recommended.
3. Calibrate the software by analyzing several frames of the video to appropriately determine selection and rejection parameters (size, bandpass, etc) for identifying probe center positions. Extensive background for these crucial steps is described by Crocker and Grier.
4. Use the software to automatically determine each probe position for all video frames and then link these positions into trajectories.
5. Use the trajectory data to compute the mean squared displacement (MSD) as a function of lag time, being sure to apply the appropriate spatial calibration factor (μm per pixel) for the specific objective lens, any pixel binning, etc (typically carried in meta-data).
6. Calculate G*(using the generalized Stokes-Einstein relation taken into consideration the limits of applicability of GSER for a particular sample[24,28,43]. Alternatively, users may wish to interpret ECM properties directly from MSD by simply comparing power law scaling, plateau values, indices of heterogeneity or other parameters.
7. Repeat steps 4.2 through 4.6 for each fov in the experiment.
8. Co-register position data from step 3.4 with viscoelastic modulii at a particular frequency of interest. Depending on the manufacturer of the microscope used, this step can be facilitated by a custom routine which reads microscope metadata or position data can be tabulated manually.
9. Use 3D interpolation functions to generate a spatial rheology map of the ECM.

Representative Results

To verify the validity of *G*(ω)* measurements at localized positions within a complex model tumor microenvironment, two initial validation experiments were conducted. First, we sought to validate our measurements against the "gold standard" of bulk oscillatory shear rheometry. We prepared identical samples of collagen matrix (without cells) at a concentration of 1.0 mg/ml collagen. These samples were probed with a bulk rheometer (TA Instruments AR-G2, using 40 mm parallel plate geometry) and by PTM (using the same parameters as throughout this protocol) and the resulting measurements of G'(ω) and G" (ω) were compared (**Figure 2A**). Excellent agreement was found between the two measurements. Secondly, to establish the ability of this protocol to measure point changes in ECM rheology we prepared a 1.0 mg/ml collagen matrix and embedded tracer beads. The sample was then treated with a centralized injection of 5 μl dispase (**Figure 2B**), which rapidly digests collagen. After incubating for 3 hr to allow localized collagen digestion to occur, video data was taken at varying distances from the injection site, and measurements of G'(ω) and G"(ω) were made in each case. The magnitude of G"(ω = 1 rad/sec) was found to be larger than that of G'(ω = 1 rad/sec) at the injection site. Measurements taken at increasing distances from the injection site were found to have an increasing magnitude of G*, as well as an increasing ratio of G' to G" (**Figure 2C**). The size of the highly degraded region of ~2 mm is consistent with an estimated distance of diffusion of a protein with hydrodynamic radius R_H = 1 nm (the molecular weight of dispase is 32.5 kDa) through digested collagen with viscosity of η = 10^{-3} Pa·sec at 37 °C: $\Delta x = \sqrt{2D\Delta t} = 2.2\times10^{-3} m$, where $D = \frac{kT}{6\pi\eta R_H}$. Therefore the results agree with the expected softening of the matrix near the injection site, and demonstrate our ability to make accurate, localized measurements of matrix rheology.

Representative data from a 3D tumor model prepared according to this protocol is shown in **Figure 3**. Video data was collected at 19 fixed locations within the collagen scaffold, forming a rough grid around the tumor (**Figure 3A**). This coordinate data was combined with calculated values of G'(ω) to create a spatial map of ECM stiffness (**Figure 3B**). This spatial map clearly reveals a zone of heightened rigidity immediately proximal to the tumor spheroid at day 2, which could be correlated with the deposition of collagen IV, laminin V and other basement membrane components deposited by the spheroid itself[17,18,44,45], or local compression of the ECM by the expanding spheroid.

Tumor growth and matrix invasion events were monitored over 4 days. Two regions were identified as having either no evidence of invasive cells at the tumor periphery, or pronounced evidence of invading cells (**Figure 3C**). PTM measurements were taken at regions 1 and 2 over 4 days. By day 4, there was a significant difference in G' (reported at 1 rad/sec) between the two regions (**Figure 3D**). Frequency-dependent measurements of G' and G" for regions 1 and 2 on day 4 show significant softening of the ECM at region 2, the invasive region (**Figure 3E**). On day 4 region two exhibits a liquid-like viscoelastic response, evident by viscous scaling of the G" plot (**Figure 3E**).

Representative sub-optimal results from common experimental and analysis errors are shown in **Figure 4**. Perhaps the most obvious source of error lies in the stability of the setup on which video microscopy is performed. If the lab bench is displaced or if there is some other external source of vibration, bead trajectories can be artificially influenced, which results in a drift in the data. Drift causes the MSD to increase dramatically at high lag times (**Figure 4A**) which also causes the G'(ω) and G"(ω) calculated values to increase sharply at low frequencies (**Figure 4B**). Drift can be reduced through the use of a pneumatic, air cushioned lab bench, and by simply taking care to not bump the setup while videos are being recorded. Additionally, drift may be removed during post processing using software routines. These routines are suitable for removing drift which is approximately uniform over a known time interval. Erratic drift (perhaps caused by bumping the stage during data acquisition) is more problematic. Therefore it is important to make sure that the sample remains mechanically isolated from the environment during data collection.

Another potential source of unclear results comes from improper interpretation of sample heterogeneity. Although the ability to observe and quantify spatial heterogeneity in a sample is indeed one of the noted strengths of PTM[26] (and something that is lost in traditional bulk rheology measurements), improper grouping of clusters of probe trajectories can lead to incorrect conclusions. Given that changes in ECM rigidity reported by this methodology are inherently heterogeneous, as is the material itself, in any given field of view, there could be a few tracer probes that are not elastically confined by collagen fibers and thus free to stochastically explore larger water-filled pores (**Figure 4C**). These "loose" probes exhibit mobility approximately consistent with a purely viscous environment. Since data for all probes is averaged before viscoelastic moduli are calculated, having a few loose probes in a given sampling region (field of view) can produce frequency dependent plots of G*(ω) that vary wildly (**Figure 4D**).

Improper software calibration can lead to errors during video collection and analysis. During video data collection, it is important to observe the intensity histogram and adjust the exposure time to give the greatest dynamic range possible while ensuring that the image does not become saturated. The analysis computes refined center positions for each tracer probe by integrating the intensity value of each pixel. If the image is saturated, this integration will be less accurate due to a 'flat top' section of the intensity profile. Additionally, the feature finding calibration is an extremely critical step in ensuring accurate results. Proper choice of selection parameters is paramount. This process has been described extensively by Crocker and Grier[42], Savin and Doyle[43], and others.

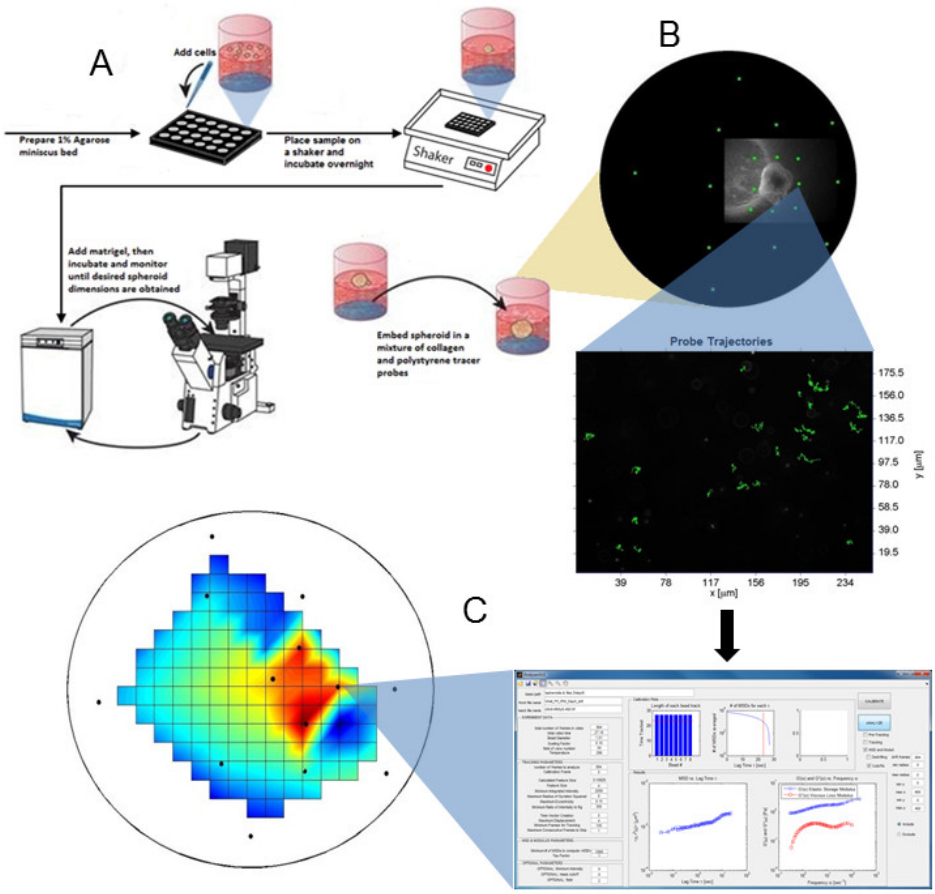

Figure 1. Schematic of Experimental Procedure. (**A**) Tumor spheroids are formed on agarose beds, and then transferred into a 3D matrix containing embedded tracer probes. (**B**) Video data is taken at several points within the sample well, both adjacent to and far away from the tumor spheroid. (**C**) The stochastic motion of the probes in each video is analyzed in order to determine the local rheological properties of the matrix at each sample point. This data is compiled into a spatial mapping of ECM stiffness throughout the well. Please click here to view a larger version of this figure.

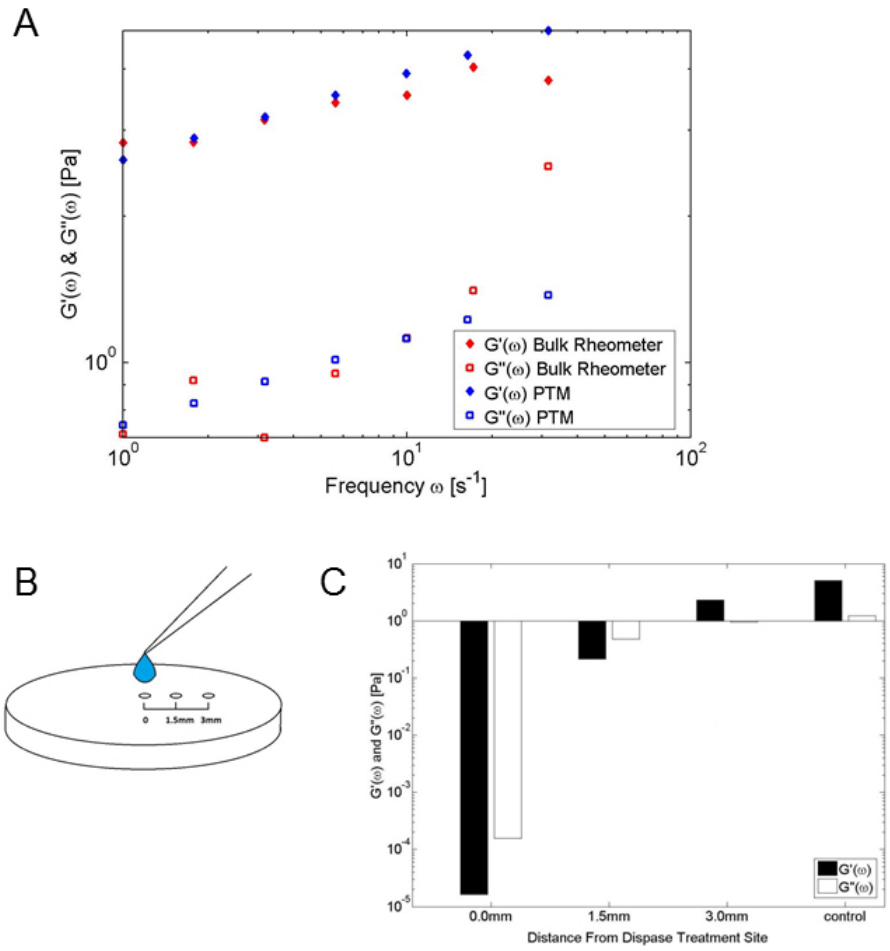

Figure 2. Verification of Measurements.(**A**) The components of G*(ω) are shown here. The calculated values of G'(ω) and G"(ω) using PTM are very similar to those obtained via a bulk rheometer. (**B**) 5 µl of dispase was added to the center of a well with radius r = 8.5 mm containing 1.0 mg/ml collagen to measure spatial changes in G*(ω). (**C**) Calculated values of G'(ω) and G"(ω) at the site of the dispase injection, 1.5 mm from the site, and 3 mm from the site. Additionally, a control measurement was made in a well containing the same collagen gel but with no dispase treatment. Near the treatment site G'(ω) is smaller than G"(ω). As the gel is sampled further from the treatment site the values of G'(ω) become larger than G"(ω), and the magnitude of G*(ω) increases. Measurements were taken 2.5 hr after dispase injection. Please click here to view a larger version of this figure.

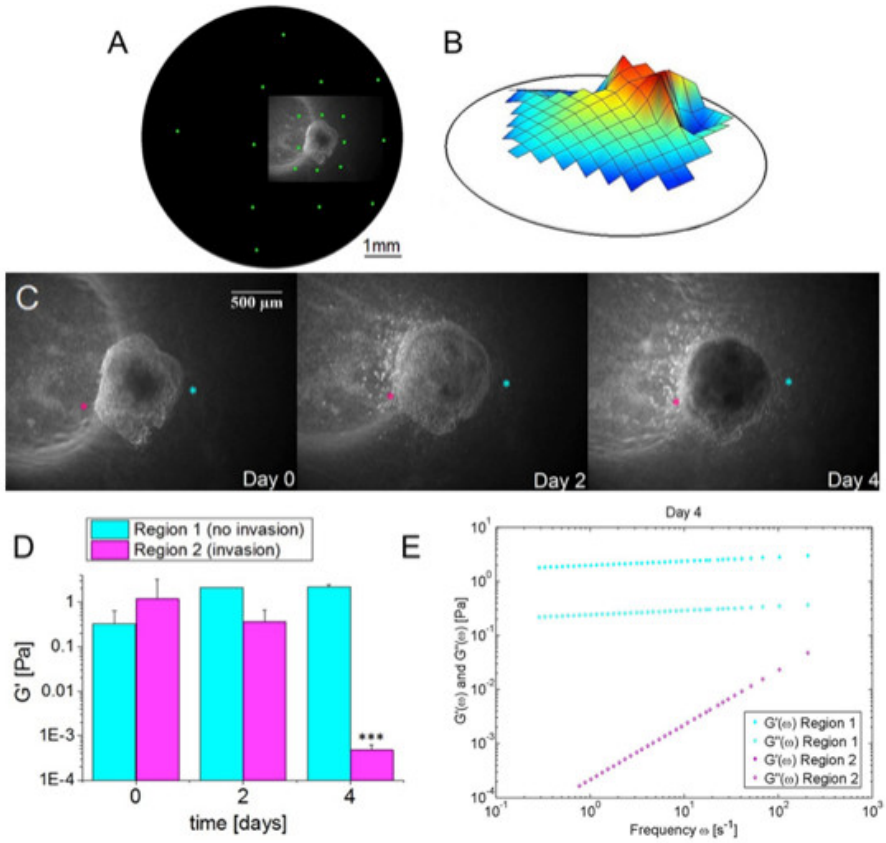

Figure 3. Quantifying changes in ECM rheology concomitant with onset of local matrix invasion. (**A**) The well containing a PANC-1 3D spheroid is probed at multiple locations throughout the collagen ECM surrounding the tumor. (**B**) Coordinate data is combined with calculated G'(ω) for each location to produce a spatial ECM rigidity map. (**C**) Tumor growth and invasion behavior were monitored over 4 days. Two regions were identified as having either no interaction with invading cells (region 1, blue asterisk) or heavy interaction with invading cells which spontaneously branched out from the large primary multicellular spheroid mass (region 2, red asterisk). (**D**) Rheological measurements were taken at regions 1 and 2 over 4 days. By the fourth day, there was a significant difference in G' (reported at 1 rad/sec) between the two regions. (**E**) Frequency dependent measurements of G'(ω) and G"(ω) for regions 1 and 2 on day 4 show significant softening of the ECM at region 2, precisely correlated with the presence of invasive populations. G'(ω) and G"(ω) values calculated using a power law fit to MSD data are shown as filled and unfilled point respectively. On day 4, region two exhibits a liquid-like viscoelastic response as is evident by viscous scaling of the G"(ω) plot and the absence of the fit line for G'(ω). Please click here to view a larger version of this figure.

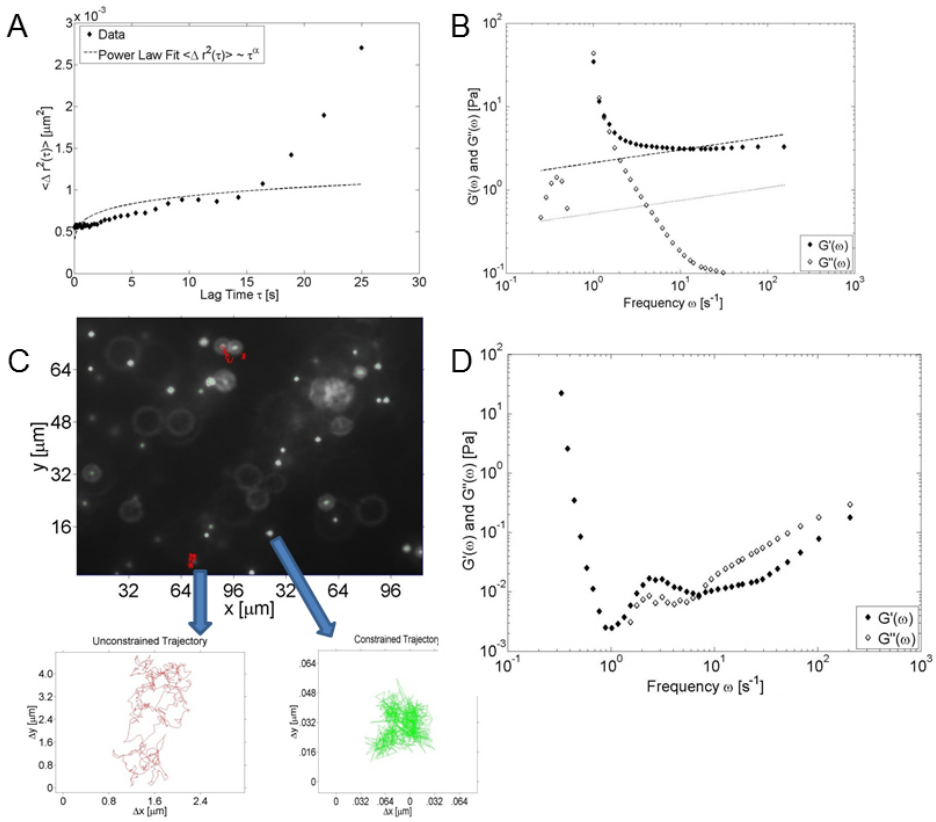

Figure 4. Data from sub-optimal results due to drift and incorrect interpretation of ECM heterogeneity. (**A**) The MSD of a tracer probe confined in a complex material follows power law scaling $<\Delta r^2(\tau)> \sim \tau^{\alpha}$ ($0 \leq \alpha \leq 1$). Accordingly, MSD values should approach a plateau at long lag times. Drift in the sample can artificially eliminate this behavior, leading to escalating MSD values at long lag times. (**B**) The long lag time drift in the MSD will cause the values of G'(ω) and G"(ω) to become significantly erroneous at short frequencies. Drift can be eliminated or reduced either by ensuring that the sample is mechanically isolated during data collection or by using software routines to remove drift during the analysis. (**C**) Even in a small field of view, two distinct varieties of probe trajectories may be present. In this example, most of the probes are confined in the matrix, but a few are 'loose' - their trajectories are much less constrained. (**D**) Attempting to interpret MSD data from both constrained and unconstrained probes at the same time without proper interpretation of sample heterogeneity will confound measurements of viscoelastic moduli. Please click here to view a larger version of this figure.

Discussion

In this protocol we introduce a robust and widely applicable strategy for longitudinally tracking local changes in ECM rigidity in 3D tumor models. We envision that this methodology could be adopted by cancer biologists and biophysicists interested in mechanosensitive behavior implicated in matrix remodeling during tumor growth and invasion processes. Precise quantification of matrix degradation kinetics could be particularly valuable to those studying the activity of matrix metalloproteases, lysyl oxidase or other relevant biochemical species in 3D tumor models that are directly linked to matrix remodeling. Beyond the application to 3D tumor models described here, one could further imagine the implementation of this approach in conjunction with other disease model systems in which modification of matrix rheology over time plays important roles[46,47]. The utility of this method continues to be enhanced through software improvements that further automate the process and allow for increased throughput studies. This will result in increasingly detailed snapshots of the physical landscape of many samples, simultaneously, for use in multi-well formats.

Here we specifically describe the implementation of passive particle-tracking microrheology in 3D tumor models, which is well suited for measurement of linear viscoelastic response in the range of ~tens of Pascal typical of commercially available extracellular matrix products (bovine collagen, EHS-tumor extracts or commercial nanofiber scaffolds). The observation of stochastic, thermally driven motion, even with high numerical aperture optics to quantify small probe displacements, is inherently limited to the linear regime of these relatively soft ECM environments, but investigators desiring to probe more rigid materials may be able to adapt this protocol for use with active manipulations via optical[48] or magnetic trapping[49] of probes. Since the optical or magnetic tweezers probe a single point within a sample and do not affect the integrity of the sample, these techniques could possibly be incorporated into the above protocol to obtain longitudinal measurements of more rigid samples.

It is important to observe that other cell generated forces may also contribute to tracer probe movements at various time scales. For example, during cell migration occurring over the course of hours and days in culture, clusters of probes will be pushed and pulled due to cell movements and it is indeed this motion that is utilized in traction force microscopy[50,51]. The thermally driven probe movements which are analyzed to obtain microrheology data take place on the order of seconds, a clearly separable time scale. While it is also true that the slower dynamics of stresses and strains associated with traction forces can contribute to local changes in rheology[36], a strength of this imaging-based approach lies in

the ability to correlate visual and rheological changes in the sample. For example in the representative results in **Figure 3**, an obvious matrix invasion and cell migration event is correlated with a change in G′ of nearly four orders of magnitude during the time this migration takes place.

The protocol described here assumes that users have access to a microscope with a motorized stage that provides reproducible positioning of the sample. Labs that do not have this instrumentation could still make point measurements using marks or other visual cues in the sample or sample carrier to allow repeated measurements at the same point, though it would likely be difficult to achieve the same reproducibility in positioning as shown in the representative longitudinal measurements here. For the purposes of these representative results above, positioning on the z-axis was kept approximately constant. However, the protocol could also be amended to include additional measurements along the z-axis in order to create a 3D rheological map of the sample. The method could also be modified to utilize a scanning laser confocal or a multiphoton techniques for 3D sectioning though scan speeds would impose a limitation on the upper frequency limits accessible that may or may not be problematic for a given application.

In this method, a significant time constraint is imposed by the necessity of returning live cells to the incubator. Without a time-lapse weather station enclosure to control for temperature, humidity, and CO_2 levels, image acquisition time must be minimized. Even with the proper equipment, data collection takes up large amounts of time and digital memory, which are both subject to practical limitations. For instance, with microscope and camera used in this study, it would take roughly 35 hr to take the roughly 4,000 videos necessary to map a single well on a 96-well plate using a 100X objective lens with no space between fields of view. These factors impose constraints on the number of data points that can realistically be collected. The level of detail is, therefore subject to the practical constraints imposed by time available for data collection, data storage space and the availability of an environmental housing.

The ability to quantify changes in ECM rheology could be further integrated alongside imaging-based methods for quantification of therapeutic response in 3D tumor models[17,18,52,53]. The multi-well 3D model culture system adopted in both methods suggests a parallel implementation providing correlation between cytotoxic response and modification of the mechanical environment. This could facilitate development of further strategies that explicitly target the mechanical phenotype or elucidate the impact of existing therapeutics in this capacity. Such insight could be directly relevant to approaches to enhance drug delivery through dense collagen-rich tumor stroma. For example, in the context of the representative illustration of this protocol presented here with *in vitro* pancreatic tumor models, the evaluation of matrix degradation following interventions could be used in screening stromal depletion regimens, an increasingly important therapeutic paradigm for pancreatic cancer[54].

Disclosures

The authors declare that they have no competing financial interests.

Acknowledgements

We gratefully acknowledge the open-source sharing of MATLAB particle-tracking code provided by Maria Kilfoil (http://people.umass.edu/kilfoil/), along with the earlier IDL code and extensive documentation provided by John C. Crocker and Eric R. Weeks. This work was made possible by funding from the National Cancer Institute (NCI/NIH), K99CA155045 and R00CA155045 (PI: JPC).

References

1. Bissell, M. J. *et al.* Tissue structure, nuclear organization, and gene expression in normal and malignant breast. *Cancer Res.* **59**, 1757-1763s; discussion 1763s-1764s (1999).
2. Kumar, S., & Weaver, V. M. Mechanics, malignancy, and metastasis: the force journey of a tumor cell. *Cancer metastasis reviews.* **28**, 113-127, doi:10.1007/s10555-008-9173-4 (2009).
3. Paszek, M. J. *et al.* Tensional homeostasis and the malignant phenotype. *Cancer cell.* **8**, 241-254, doi:10.1016/j.ccr.2005.08.010 (2005).
4. Bershadsky, A. D., Balaban, N. Q., & Geiger, B. Adhesion-dependent cell mechanosensitivity. *Annual review of cell and developmental biology.* **19**, 677-695, doi:10.1146/annurev.cellbio.19.111301.153011 (2003).
5. Dupont, S. *et al.* Role of YAP/TAZ in mechanotransduction. *Nature.* **474**, 179-183, doi:10.1038/nature10137 (2011).
6. Ingber, D. E. Tensegrity-based mechanosensing from macro to micro. *Prog Biophys Mol Biol.* **97**, 163-179, doi:10.1016/j.pbiomolbio.2008.02.005 (2008).
7. Peyton, S. R., Ghajar, C. M., Khatiwala, C. B., & Putnam, A. J. The emergence of ECM mechanics and cytoskeletal tension as important regulators of cell function. *Cell Biochem Biophys.* **47**, 300-320, doi:CBB:47:2:300 [pii] (2007).
8. Schmeichel, K. L., & Bissell, M. J. Modeling tissue-specific signaling and organ function in three dimensions. *J Cell Sci.* **116**, 2377-2388 (2003).
9. Nelson, C. M., & Bissell, M. J. Of extracellular matrix, scaffolds, and signaling: tissue architecture regulates development, homeostasis, and cancer. *Annu Rev Cell Dev Biol.* **22**, 287-309 (2006).
10. Butcher, D. T., Alliston, T., & Weaver, V. M. A tense situation: forcing tumour progression. *Nat Rev Cancer.* **9**, 108-122, doi:10.1038/nrc2544 (2009).
11. Assoian, R. K., & Klein, E. A. Growth control by intracellular tension and extracellular stiffness. *Trends Cell Biol.* **18**, 347-352, doi:10.1016/j.tcb.2008.05.002 (2008).
12. Lee, G. Y., Kenny, P. A., Lee, E. H., & Bissell, M. J. Three-dimensional culture models of normal and malignant breast epithelial cells. *Nat Methods.* **4**, 359-365 (2007).
13. Debnath, J., & Brugge, J. S. Modelling glandular epithelial cancers in three-dimensional cultures. *Nature reviews. Cancer.* **5**, 675-688, doi:10.1038/nrc1695 (2005).
14. Ulrich, T. A., Jain, A., Tanner, K., MacKay, J. L., & Kumar, S. Probing cellular mechanobiology in three-dimensional culture with collagen-agarose matrices. *Biomaterials.* **31**, 1875-1884, doi:10.1016/j.biomaterials.2009.10.047 (2010).

15. Abu-Yousif, A. O., Rizvi, I., Evans, C. L., Celli, J. P., & Hasan, T. PuraMatrix encapsulation of cancer cells. *J. Vis. Exp.* (34), doi:10.3791/1692 (2009).
16. Debnath, J., Muthuswamy, S. K., & Brugge, J. S. Morphogenesis and oncogenesis of MCF-10A mammary epithelial acini grown in three-dimensional basement membrane cultures. *Methods.* **30**, 256-268 (2003).
17. Celli, J. P., Rizvi, I., Evans, C. L., Abu-Yousif, A. O., & Hasan, T. Quantitative imaging reveals heterogeneous growth dynamics and treatment-dependent residual tumor distributions in a three-dimensional ovarian cancer model. *J Biomed Opt.* **15**, 051603-051610 (2010).
18. Rizvi, I. *et al.* Synergistic Enhancement of Carboplatin Efficacy with Photodynamic Therapy in a Three-Dimensional Model for Micrometastatic Ovarian Cancer. *Cancer Res.* **70**, 9319-9328, doi:10.1158/0008-5472.can-10-1783 (2010).
19. Cretu, A., Castagnino, P., & Assoian, R. Studying the Effects of Matrix Stiffness on Cellular Function using Acrylamide-based Hydrogels. *J. Vis. Exp.* (42), e2089, doi:doi:10.3791/2089 (2010).
20. Kenny, H. A., & Lengyel, E. MMP-2 functions as an early response protein in ovarian cancer metastasis. *Cell Cycle.* **8**, doi:7703 [pii] (2009).
21. Kenny, H. A., Kaur, S., Coussens, L. M., & Lengyel, E. The initial steps of ovarian cancer cell metastasis are mediated by MMP-2 cleavage of vitronectin and fibronectin. *J Clin Invest.* **118**, 1367-1379, doi:10.1172/JCI33775 (2008).
22. Lee, J. M., Dedhar, S., Kalluri, R., & Thompson, E. W. The epithelial-mesenchymal transition: new insights in signaling, development, and disease. *J Cell Biol.* **172**, 973-981, doi:10.1083/jcb.200601018 (2006).
23. Mason, T. G., & Weitz, D. A. Optical Measurements of Frequency-Dependent Linear Viscoelastic Moduli of Complex Fluids. *Physical Review Letters.* **74**, 1250 (1995).
24. Mason, T. G., Ganesan, K., van Zanten, J. H., Wirtz, D., & Kuo, S. C. Particle Tracking Microrheology of Complex Fluids. *Physical Review Letters.* **79**, 3282-3285 (1997).
25. Crocker, J. C. *et al.* Two-Point Microrheology of Inhomogeneous Soft Materials. *Physical Review Letters.* **85**, 888 (2000).
26. Valentine, M. T. *et al.* Investigating the microenvironments of inhomogeneous soft materials with multiple particle tracking. *Physical Review E.* **64**, 061506 (2001).
27. Helfer, E. *et al.* Microrheology of Biopolymer-Membrane Complexes. *Physical Review Letters.* **85**, 457 (2000).
28. Levine, A. J., & Lubensky, T. C. One- and Two-Particle Microrheology. *Physical Review Letters.* **85**, 1774 (2000).
29. Jonas, M., Huang, H., Kamm, R. D., & So, P. T. Fast fluorescence laser tracking microrheometry, II: quantitative studies of cytoskeletal mechanotransduction. *Biophys J.* **95**, 895-909, doi:S0006-3495(08)70264-9 [pii] biophysj.107.120303 (2008).
30. Celli, J. *et al.* Viscoelastic properties and dynamics of porcine gastric mucin. *Biomacromolecules.* **6**, 1329-1333, doi:10.1021/bm0493990 (2005).
31. Pelletier, V., Gal, N., Fournier, P., & Kilfoil, M. L. Microrheology of microtubule solutions and actin-microtubule composite networks. *Phys Rev Lett.* **102**, 188303 (2009).
32. Bloom, R. J., George, J. P., Celedon, A., Sun, S. X., & Wirtz, D. Mapping local matrix remodeling induced by a migrating tumor cell using three-dimensional multiple-particle tracking. *Biophys J.* **95**, 4077-4088, doi:S0006-3495(08)78545-X [pii] biophysj.108.132738 (2008).
33. Gordon, V. D. *et al.* Measuring the mechanical stress induced by an expanding multicellular tumor system: a case study. *Exp Cell Res.* **289**, 58-66, doi:S0014482703002568 [pii] (2003).
34. Li, Y., Schnekenburger, J., & Duits, M. H. Intracellular particle tracking as a tool for tumor cell characterization. *J Biomed Opt.* **14**, 064005, doi:10.1117/1.3257253 (2009).
35. Tseng, Y., Kole, T. P., & Wirtz, D. Micromechanical Mapping of Live Cells by Multiple-Particle-Tracking Microrheology. *Biophysical Journal.* **83**, 3162-3176, doi:http://dx.doi.org/10.1016/S0006-3495(02)75319-8 (2002).
36. Gjorevski, N., & Nelson, Celeste M. Mapping of Mechanical Strains and Stresses around Quiescent Engineered Three-Dimensional Epithelial Tissues. *Biophysical Journal.* **103**, 152-162, doi:http://dx.doi.org/10.1016/j.bpj.2012.05.048 (2012).
37. Yang, Y. L., Motte, S., & Kaufman, L. J. Pore size variable type I collagen gels and their interaction with glioma cells. *Biomaterials.* **31**, 5678-5688, doi:10.1016/j.biomaterials.2010.03.039 (2010).
38. Ludwig, T., Kirmse, R., Poole, K., & Schwarz, U. S. Probing cellular microenvironments and tissue remodeling by atomic force microscopy. *Pflugers Archiv : European journal of physiology.* **456**, 29-49, doi:10.1007/s00424-007-0398-9 (2008).
39. Sipos, B. *et al.* A comprehensive characterization of pancreatic ductal carcinoma cell lines: towards the establishment of an *in vitro* research platform. *Virchows Archiv : an international journal of pathology.* **442**, 444-452 (2003).
40. Timmins, N. E., & Nielsen, L. K. Generation of multicellular tumor spheroids by the hanging-drop method. *Methods Mol Med.* **140**, 141-151 (2007).
41. Kim, J. B. Three-dimensional tissue culture models in cancer biology. *Semin Cancer Biol.* **15**, 365-377 (2005).
42. Crocker, J. C., & Grier, D. G. Methods of Digital Video Microscopy for Colloidal Studies. *Journal of Colloid and Interface Science.* **179**, 298-310, doi:http://dx.doi.org/10.1006/jcis.1996.0217 (1996).
43. Savin, T., & Doyle, P. S. Static and Dynamic Errors in Particle Tracking Microrheology. *Biophysical Journal.* **88**, 623-638, doi:http://dx.doi.org/10.1529/biophysj.104.042457 (2005).
44. Evans, C. L. *et al.* Killing hypoxic cell populations in a 3D tumor model with EtNBS-PDT. *PLoS ONE.* **6**, e23434, doi:10.1371/journal.pone.0023434 (2011).
45. Debnath, J. *et al.* The role of apoptosis in creating and maintaining luminal space within normal and oncogene-expressing mammary acini. *Cell.* **111**, 29-40 (2002).
46. Celli, J. P. *et al.* Helicobacter pylori moves through mucus by reducing mucin viscoelasticity. *Proc Natl Acad Sci U S A.* **106**, 14321-14326, doi:0903438106 [pii] pnas.0903438106 (2009).
47. Bansil, R., Celli, J. P., Hardcastle, J. M., & Turner, B. S. The Influence of Mucus Microstructure and Rheology in Helicobacter pylori Infection. *Frontiers in immunology.* **4**, 310, doi:10.3389/fimmu.2013.00310 (2013).
48. Furst, E. M. Applications of laser tweezers in complex fluid rheology. *Current Opinion in Colloid & Interface Science.* **10**, 79-86, doi:http://dx.doi.org/10.1016/j.cocis.2005.04.001 (2005).
49. Gosse, C., & Croquette, V. Magnetic Tweezers: Micromanipulation and Force Measurement at the Molecular Level. *Biophysical Journal.* **82**, 3314-3329, doi:http://dx.doi.org/10.1016/S0006-3495(02)75672-5 (2002).
50. Dembo, M., & Wang, Y.-L. Stresses at the Cell-to-Substrate Interface during Locomotion of Fibroblasts. *Biophysical Journal.* **76**, 2307-2316, doi:http://dx.doi.org/10.1016/S0006-3495(99)77386-8 (1999).
51. Franck, C., Maskarinec, S. A., Tirrell, D. A., & Ravichandran, G. Three-dimensional traction force microscopy: a new tool for quantifying cell-matrix interactions. *PLoS ONE.* **6**, e17833 (2011).

52. Celli, J. P., Petrovic, L., Massdodi, I., Rizvi, I., & Hasan, T. Overcoming therapeutic resistance in pancreatic cancer is not a simple mix of PDT and chemotherapy: Evaluation of PDT-chemotherapy combinations in 3D tumor models. *Proc SPIE.* 85680R-85680R, doi:10.1117/12.2010730 (2013).
53. Glidden, M. D. *et al.* Image-Based Quantification of Benzoporphyrin Derivative Uptake, Localization, and Photobleaching in 3D Tumor Models, for Optimization of PDT Parameters. *Theranostics.* **2**, 827-839, doi:10.7150/thno.4334 (2012).
54. Celli, J. P. *et al.* An imaging-based platform for high-content, quantitative evaluation of therapeutic response in 3D tumour models. *Scientific reports.* **4**, 3751, doi:10.1038/srep03751 (2014).
55. Celli, J. P. Stromal interactions as regulators of tumor growth and therapeutic response: A potential target for photodynamic therapy? *Israel journal of chemistry.* **52**, 757-766, doi:10.1002/ijch.201200013 (2012).
56. Garber, K. Stromal depletion goes on trial in pancreatic cancer. *J Natl Cancer Inst.* **102**, 448-450, doi:10.1093/jnci/djq113 (2010).

